Construction and Building Materials 365 (2023) 129924

Contents lists available at ScienceDirect

Construction and Building Materials

journal homepage: www.elsevier.com/locate/conbuildmat

Estimating the diameter of reinforcing bars using an ultra-wideband MIMO GPR array

Weixia Cheng [a,1], Hai-Han Sun [a,1], Kang Hai Tan [b,*], Zheng Fan [a,*]

[a] School of Mechanical and Aerospace Engineering, Nanyang Technological University, 50 Nanyang Avenue, Singapore
[b] School of Civil and Environmental Engineering, Nanyang Technological University, 50 Nanyang Avenue, Singapore

ARTICLE INFO

Keywords:
Diffraction stacking algorithm
Ground-penetrating radar
Multiple-input-multiple-output (MIMO) array
Non-destructive inspection
Reinforcing bar

ABSTRACT

Ground-penetrating radar (GPR) is an effective non-destructive detection technology for locating and characterizing reinforcing bars in concrete structures. However, the accurate quantification of reinforcing bar diameters, especially in small-diameter cases, remains a challenging issue. In this paper, a sizing method based on multiple-input-multiple-output (MIMO) GPR arrays is presented to estimate the reinforcing bar diameter in concrete. The method employs a linear array of ultra-wideband (UWB) antennas to acquire the full-matrix MIMO data of the reinforcing bar embedded in concrete. The diffraction stacking algorithm is applied to the obtained MIMO data to reconstruct the reinforcing bar. The 3 decibels (dB) drop technique is used to measure the chord length that passes through the peak intensity point of the reconstruction image of the reinforcing bar. Following that, the diameter of the reinforcing bar can be determined based on its cover depth and the chord length. Extensive numerical studies and experiments have been conducted to examine the performance of the proposed method in different scenarios. The method shows excellent sizing accuracy for reinforcing bars with different diameters and cover depths.

1. Introduction

Cross-section reduction of reinforcing bars induced by corrosion has a direct impact on the durability and sustainability of reinforced concrete (RC) structures [1–4]. Accurate measurement of reinforcing bar diameter is therefore of paramount importance for the health examination and safety evaluation of the concrete structures [5]. Ground-penetrating radar (GPR), based on electromagnetic wave propagation and reflection, has been effectively implemented to detect and locate subsurface reinforcing bars in concrete due to the great contrast of permittivity between concrete and reinforcing bars [6–9]. However, accurately estimating reinforcing bar diameters remains a challenging issue for the existing GPR techniques.

Several methods have been proposed to estimate the diameter of cylindrical objects using GPR data. As the hyperbolic geometry reflected by cylindrical objects in B-scans contains information of object parameters, pattern-based methods including curve-fitting techniques [10–13] and generalized Hough transform algorithms [14–16] were developed to estimate the diameter based on the hyperbolic arc. The methods can estimate cylindrical objects with diameters larger than 20 mm with good accuracy [11]. However, they are ineffective in quantifying cylindrical objects with diameters smaller than the GPR working wavelength [17,18]. To size the small-diameter reinforcing bars, dual-polarization methods were proposed based on the difference of radar cross-section of cylindrical bars on orthogonal polarizations [19–21]. They use the ratio of the amplitudes of orthogonal polarizations to estimate the diameter of the reinforcing bars. However, the method has not been well established to take into account of different GPR operating frequencies and subsurface permittivity values, so it is still challenging to be accurately used in real situations. Full-waveform inversion (FWI) was applied to extract the size of reinforcing bars with an error of less than 11% [17], but its large amount of computational cost limits its applicability in real-time in-situ subsurface examination. To obtain characteristics of reinforcing bars in real-time, machine learning (ML)-based algorithms have been developed [18,22,23]. The algorithms establish the relationship between radar data and reinforcing bar parameters by training with a large amount of paired data. The applicability and the accuracy of the ML-based algorithms in different subsurface scenarios heavily depend on the training dataset.

Multiple-input-multiple-output (MIMO) GPR arrays have been adopted to improve the detection accuracy of subsurface objects [24–27]. Different migration algorithms have been implemented to MIMO GPR data to reconstruct subsurface objects. These migration algorithms

* Corresponding authors.
E-mail addresses: ckhtan@ntu.edu.sg (K.H. Tan), ZFAN@ntu.edu.sg (Z. Fan).
[1] The first two authors contributed equally to this work.

https://doi.org/10.1016/j.conbuildmat.2022.129924
Received 30 August 2022; Received in revised form 17 November 2022; Accepted 27 November 2022
Available online 15 December 2022

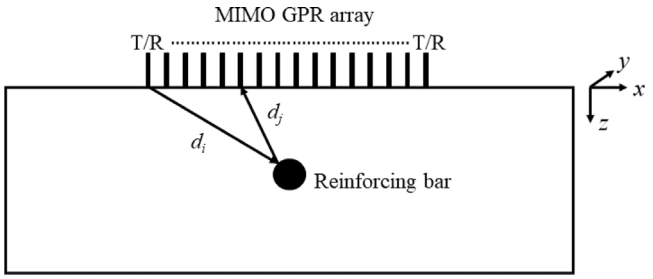

Fig. 1. Schematic of MIMO GPR array inspection of reinforcing bar in a concrete structure.

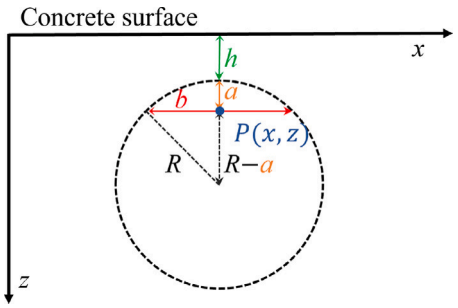

Fig. 2. Schematic diagram of the sizing method for reinforcing bar.

include the diffraction stacking migration [28–30], the Kirchhoff migration [31,32], the phase-shift migration [32], the F-K migration [32,33], and the reverse time migration [34,35]. Their imaging results demonstrate that the MIMO array configuration greatly improves the image resolution and reduces side-lobe levels compared with the conventional single-input single-output (SISO) GPR [24,26,32]. However, to the best of our knowledge, the combination of MIMO GPR arrays and imaging methods has never been investigated for sizing subsurface targets.

In this paper, we present a method for sizing reinforcing bars based on MIMO GPR arrays. In this method, a linear array of ultra-wideband (UWB) antennas is used to acquire the full-matrix MIMO data. The diffraction stacking algorithm is applied to the full-matrix MIMO data to image the reinforcing bars in concrete. From the reconstructed image, the length of the chord that passes through the peak intensity point is measured using a 3 decibels (dB) drop technique. The diameter of the reinforcing bar is then calculated based on the cover depth and the chord length. To the authors' knowledge, this is the first time that MIMO arrays are used to estimate the size of subsurface objects in the GPR field. The promising results obtained in the study can provide guidance for the use of MIMO GPR arrays to size subsurface objects in different applications.

The rest of the paper is arranged as follows. Section 2 describes the details of the proposed method. Section 3 presents the performance of the method in numerical simulations. The simulated scenarios include reinforcing bars of different diameters, cover depths, and spacing. In Section 4, experiments are conducted to evaluate the performance of the method in real cases. Finally, the conclusion is drawn in Section 5.

2. Methodology

2.1. MIMO GPR imaging using diffraction stacking algorithm

The experimental scenario of using an MIMO GPR array to detect the reinforcing bar in concrete is shown in Fig. 1. A linear array with N y-polarized antennas is placed on the concrete surface at $z = 0$. Each antenna serves as both the transmitter and receiver. The antennas transmit signals sequentially, and the signals received by all antennas are collected to obtain the $N \times N$ full-matrix MIMO data.

The diffraction stacking algorithm is an imaging technique that sums the acquired signals at different positions based on the time of flight [28]. The intensity I at each pixel position (x, z) of the image represents the amplitude of the summed signal, which is calculated by

$$I(x,z) = \left| \sum_{i=1}^{N} \sum_{j=1}^{N} S_{ij}\left(\frac{d_i + d_j}{v}\right) \right| = \left| \sum_{i=1}^{N} \sum_{j=1}^{N} S_{ij}\left(\frac{\sqrt{(x_i - x)^2 + z^2} + \sqrt{(x_j - x)^2 + z^2}}{v}\right) \right|, \quad (1)$$

where N denotes the number of transmitter and receiver; S_{ij} represents the complex signal in the time domain that is transmitted by antenna i and received by antenna j; d_i and d_j are the distance from the transmitter to the pixel position (x, z) and the distance from the pixel position (x, z) to the receiver, respectively; x_i is the x-coordinate of the transmitting antenna i and x_j is the x-coordinate of the receiving antenna j; v denotes the propagation velocity of electromagnetic waves in the concrete that is calculated by $v = c/\sqrt{\varepsilon_r}$, where c stands for the speed of light and ε_r is the relative permittivity of the concrete.

Prior to imaging, the acquired $N \times N$ MIMO data should be preprocessed. Time delay correction is carried out to compensate for time delays through cables and from the antenna feeding point to the antenna phase centre. Background subtraction is performed to eliminate the direct coupling between antennas and the reflection of concrete surface [29].

2.2. Sizing method for reinforcing bars

It is challenging to directly size the reinforcing bar from the diffraction stacking image due to the limit of resolution. In this study, we adopt the 3 decibels (dB) drop technique to estimate the diameter of the reinforcing bar from the reconstruction image. It is well-known that an antenna beam width is generally determined by the half power value, also called −3 dB point [36]. The defect smaller than the width can be assumed to be a radiator, which tends to emit everywhere inside the beam. Similar approach has also been applied in the area of ultrasonic inspection [37]. Hence, the size of the defect can be measured as the distance between −3 dB of the reconstruction image.

It should be noted that the diameter cannot be measured directly using the 3 dB drop technique. This is because a linear antenna array at a fixed position on top of the reinforcing bar has a limited viewing range and the metal bar is a total reflector. Hence, only the upper part of the bar can be imaged. Therefore, the peak intensity point of the reconstructed reinforcing bar image can only be located above the centre of the bar. Only the chord length of the reinforcing bar b passing through the peak intensity point P can be quantified directly using the 3 dB drop technique. As illustrated in Fig. 2, the chord length b will be measured as the distance between −3 dB points of the image. Given the cover depth of reinforcing bar h, which can be determined using curve fitting techniques [38], and z-coordinate of peak intensity point z_P, the height of segment a can be calculated as $a = z_P - h$. The radius of the reinforcing bar R can then be obtained by

$$(R - a)^2 + \left(\frac{b}{2}\right)^2 = R^2. \quad (2)$$

Fig. 3 outlines the flowchart of the proposed reinforcing bar sizing method based on MIMO GPR arrays.

3. Simulation validation

3.1. Simulation of the MIMO GPR array

The proposed method for reinforcing bar sizing is firstly verified in the simulated scenario. In the numerical study, gprMax2D [39,40] is

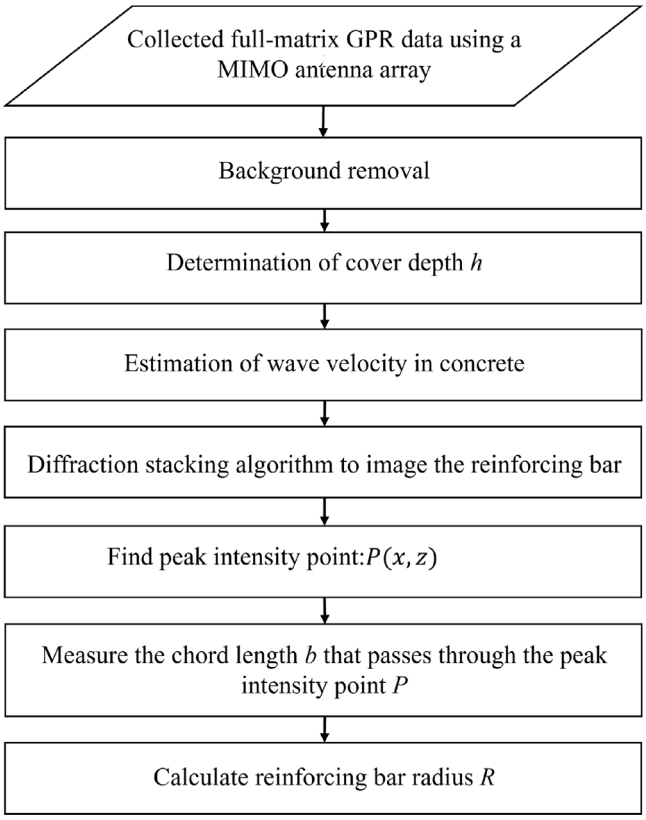

Fig. 3. Flowchart of the reinforcing bar sizing method based on MIMO GPR array.

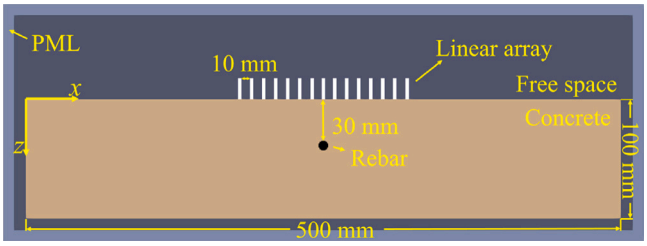

Fig. 4. Illustration of the simulation model in gprMax2D software. A reinforcing bar with a diameter of 8 mm is located at a cover depth of 30 mm in a concrete slab.

used to obtain the MIMO array data of the reinforcing bar in concrete. The simulation scenario is shown in Fig. 4. A reinforcing bar with a diameter of 8 mm is located at a cover depth of 30 mm in a concrete slab. The concrete slab has a size of 500 mm × 100 mm. The spatial discretization is 0.1 mm in the x- and z- directions, and the time step Δt is 0.236 ps. The concrete model is surrounded by an air layer of 20 mm on the lateral and bottom sides, and 80 mm on the top. A perfectly matched layer (PML) is used outside the air layer to avoid reflections from the boundary. The relative permittivity and conductivity of the concrete are set as 6 and 0.001 S/m, respectively. A linear array consisting of 15 y-polarized hertzian dipoles with a spacing of 10 mm is placed along the x-axis on the concrete surface. The array centre is aligned with the centreline of the reinforcing bar. The excitation waveform is a Ricker pulse with a central frequency at 6 GHz. Each antenna sequentially transmits radar signals and all antennas receive reflected signals, obtaining 15 × 15 full matrix MIMO GPR array data.

3.2. Validation of the reinforcing bar sizing method

The diffraction stacking algorithm is applied to the MIMO GPR data to reconstruct the reinforcing bar. The normalized imaging result is shown in Fig. 5. The black circle represents the actual size and position of the reinforcing bar. It can be seen that the reinforcing bar can be located accurately.

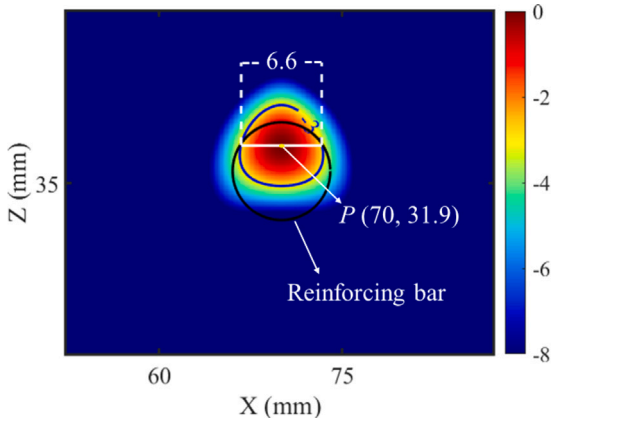

Fig. 5. The imaging result of a reinforcing bar with a diameter of 8 mm using the diffraction stacking algorithm. The peak intensity point P is positioned at z = 31.9 mm. The length of the chord passing through the point is measured as the distance between −3 dB points in the image (6.6 mm). The diameter is calculated as 7.63 mm using the proposed method.

Table 1
Sizing of reinforcing bars with different diameters and cover depths.

Cover depth (mm)	Actual diameter (mm)	Estimated diameter (mm)	Reconstruction error (%)
H30	8	7.63	4.6%
	12	12.09	0.75%
	16	17.12	7.03%
	20	21.3	6.51%
	24	25.11	4.64%
	28	29.85	6.62%
H40	8	7.72	3.46%
	12	11.11	7.4%
	16	15.82	1.1%
	20	20.49	2.44%
	24	25.27	5.3%
	28	29.18	4.23%
H50	8	8.12	1.44%
	12	11.13	7.28%
	16	15	6.25%
	20	19.53	2.37%
	24	23.36	2.68%
	28	28.82	2.95%

The 3 dB drop technique is applied to determine the chord length according to the analysis in Section 2.2. As shown in Fig. 5, the peak intensity point P is located at z = 31.9 mm, and the chord length b obtained using the 3 dB drop technique is 6.6 mm. Given the cover depth of the reinforcement h = 30 mm, the height of the segment a is calculated as 1.9 mm, and the reinforcing bar diameter is computed as 7.63 mm. It can be seen that the reinforcing bar diameter calculated using the proposed sizing method is very close to the actual diameter (8 mm).

3.3. Effect of the size and position of the reinforcing bar

Parametric study has been carried out on reinforcing bars with different diameters and located at different cover depths to further demonstrate the sizing accuracy of the proposed method. The reinforcing bar diameter varies from 8 mm to 28 mm. The cover depths are 30 mm, 40 mm, and 50 mm, respectively, which are commonly used in RC members [41]. The imaging results of the reinforcing bars with diameters of 12 mm, 20 mm, and 28 mm at different cover depths are shown in Figs. 6(a)–6(i). The white lines in the images represent the

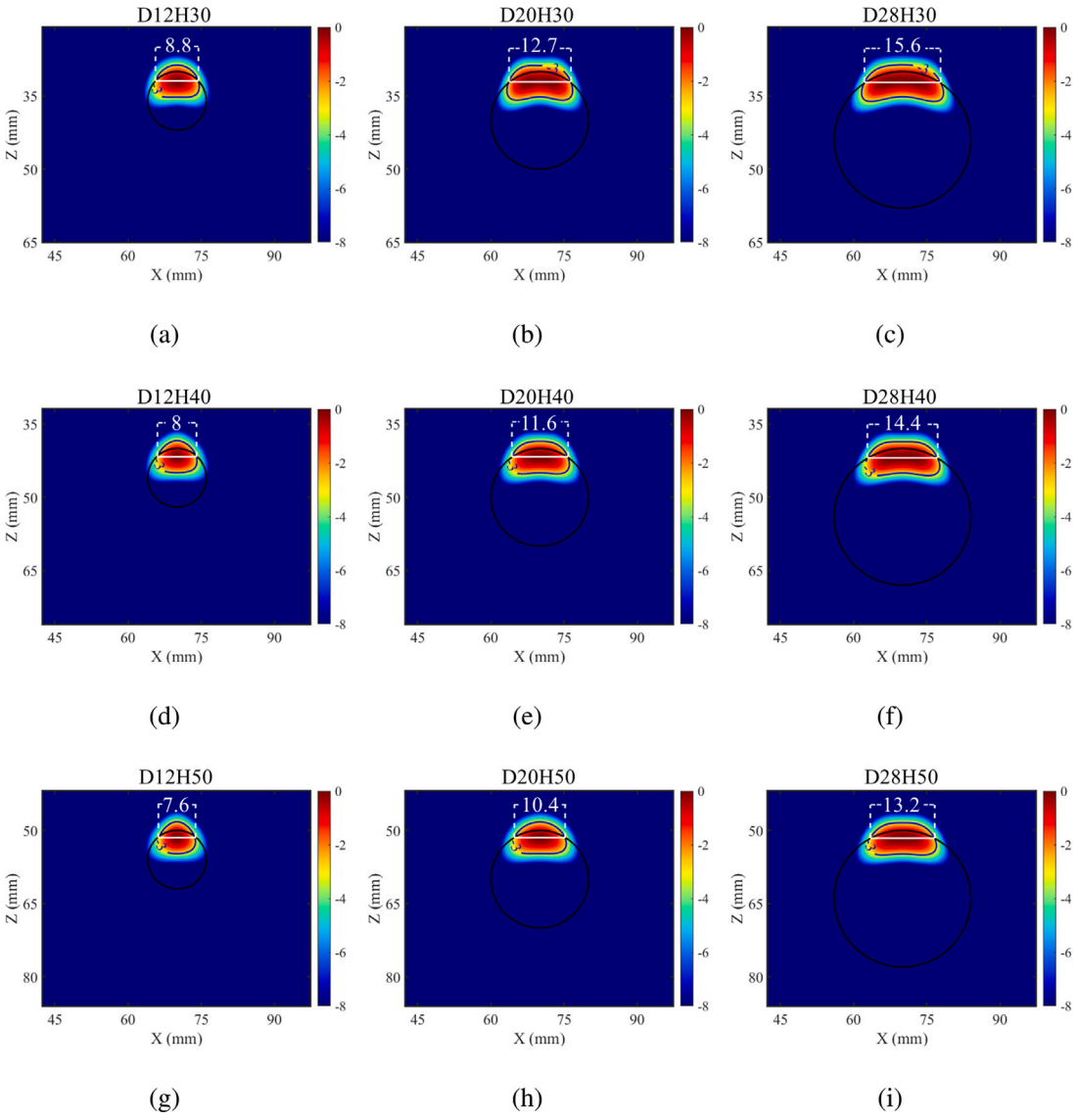

Fig. 6. Diffraction stacking migration imaging results for simulated concrete models including reinforcing bars with diameters of 12 mm, 20 mm, and 28 mm at (a)–(c) 30 mm cover depth, (d)–(f) 40 mm cover depth, and (g)–(i) 50 mm cover depth. D and H represent the diameter and the cover depth, respectively.

chord lengths that pass through the peak intensity point as measured using the 3 dB drop technique. The reinforcing bar diameters are determined based on the proposed sizing method, as listed in Table 1. It can be seen that the estimated diameter values are very close to the actual diameter values, and the percentage errors are all less than 10%. The results demonstrate that the proposed method maintains high accuracy for sizing reinforcing bars with different diameters and cover depths.

3.4. Effect of the array position

It should be noted that the sizing method requires the centre of the array to be aligned vertically with the centre of the reinforcing bar. This can be achieved experimentally by doing a B-scan imaging and identifying the centre of the hyperbolic signature [10]. However, in practice, the alignment may not be perfect each time. Hence, it would be necessary to discuss the impact of the misalignment of the array. An angle θ is used to describe the misalignment, which is between the line connecting the centres of the array and the bar with respect to the direction normal to the surface. Fig. 7 demonstrates the imaging results for an 8 mm reinforcing bar at 30 mm below the surface, with the distance l between the centre of the array and the centreline of the reinforcing bar varying from 5 mm to 20 mm. The reconstructed diameter of the reinforcing bar varies between 7.63 mm and 7.12 mm. To further illustrate the impact of the misalignment of the array, different cover depths and different array positions are investigated in a parametric study. The results are summarized in Table 2. It can be seen from the table, the reconstruction is still reasonably accurate (with an error less than 6%), when θ is smaller than 20 degree.

3.5. Effect of reinforcing bar spacing

As real reinforced concrete structures generally contain multiple reinforcing bars, it is essential to investigate the influence of reinforcing bar spacing on the sizing accuracy of the proposed method. Parametric studies have been carried out on models containing three 8 mm reinforcing bars at 30 mm depth, with spacing varying from 20 mm to 200 mm. The centre of the array is aligned with respect to the reinforcing bar in the middle. Fig. 8 illustrates imaging results for cases with the spacing of 20 mm, 60 mm, and 100 mm. Table 3 summarizes all reconstructed results for the reinforcing bar in the middle. As can be seen from the table, when the spacing between bars is small, the

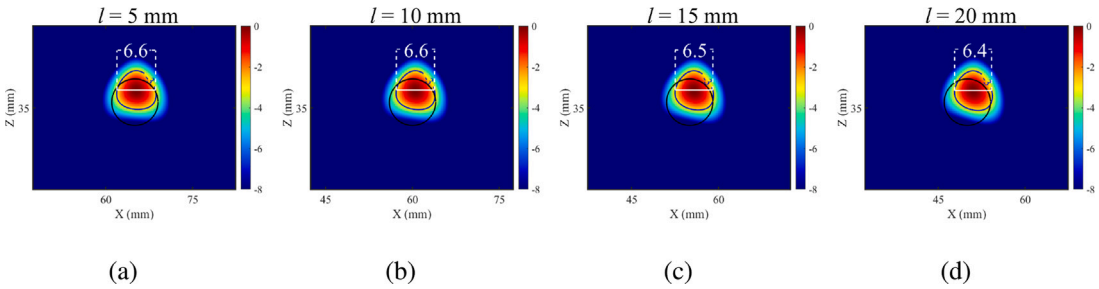

Fig. 7. Diffraction stacking migration imaging results for simulated concrete models including reinforcing bars with diameters of 8 mm at a cover depth of 30 mm. The distances between the array centre and the centreline of the reinforcing bar l are: (a) 5 mm, (b) 10 mm, (c) 15 mm, and (d) 20 mm.

Table 2
Sizing of reinforcing bars with 8 mm diameter at different array positions.

Cover depth (mm)	l (mm)	θ (°)	Estimated diameter (mm)	Reconstruction error (%)
H30	0	0	7.63	4.6%
	5	9.5	7.63	4.6%
	10	18.4	7.63	4.6%
	15	26.6	7.28	8.98%
	20	33.7	7.12	11%
	25	39.8	6.8	14.94%
	30	45	6.39	20.18%
	35	49.4	6.29	21.36%
H40	0	0	7.72	3.46%
	5	7.1	7.72	3.46%
	10	14	7.54	5.79%
	15	20.6	7.54	5.79%
	20	26.6	7.14	10.76%
	25	32	6.8	15.05%
	30	36.9	6.96	13.03%
	35	41.2	6.68	16.55%
H50	0	0	8.12	1.44%
	5	5.7	8.12	1.44%
	10	11.3	7.8	2.48%
	15	16.7	7.6	4.92%
	20	21.8	7.54	5.79%
	25	26.6	7.31	8.59%
	30	31	7.29	8.88%
	35	35	7.12	11%

Table 3
Sizing of reinforcing bar of 8 mm diameter in the case of multiple bars with different spacing.

Spacing (mm)	Estimated diameter (mm)	Reconstruction error (%)
20	10.8	35%
60	7.17	10.35%
80	7.31	8.59%
90	7.46	6.76%
100	7.63	4.61%
200	7.63	4.61%

reconstruction error could be large, due to the interference of reflected signals of adjacent reinforcing bars. As the spacing increases, such interference is reduced, leading to improved reconstruction accuracy. It should be noted that the spacing in reinforced concrete structures is usually larger than 90 mm [42,43]. Therefore, the estimation of diameter would be reasonably accurate with an error of less than 7%.

4. Experimental validation

4.1. Preparation of concrete samples

To further verify the performance of the proposed sizing method in real cases, four concrete samples are prepared, as shown in Fig. 9. Sample 1 (S#1) is prepared for investigating the sizing accuracy with different reinforcing bar diameters. As shown in Fig. 9(a), S#1 has a size of 500 mm × 130 mm × 400 mm, and has three reinforcing bars with respective diameters of 10 mm, 13 mm and 16 mm embedded in the concrete sample. The cover depths of the bars are around 30 mm with a casting tolerance of 2 mm. Samples 2–4 (S#2-S#4) are prepared for investigating the sizing accuracy with respect to different cover depths. As shown in Fig. 9(b), each of them has a size of 200 mm × 130 mm × 400 mm with an embedded 13 mm diameter reinforcing bar. The cover depths of these bars are 20 mm, 30 mm, and 40 mm, respectively. The concrete samples were cast in wood moulds and demoulded after 24 h. MIMO GPR array experiment was conducted after curing the samples for 28 days.

4.2. MIMO GPR array measurement

The MIMO GPR array system consists of a vector network analyser (Keysight VNA 5022A) and a linear antenna array, as shown in Fig. 10. The antenna array is formed by 15 y-polarization Vivaldi antennas with a spacing of 10 mm, and is assembled in a foam box. To reduce the coupling between antennas and environmental noise, the antennas are surrounded by absorbers in the box. In the experiment, the antenna array is placed on the top surface of the concrete. The middle of the array is aligned with the centreline of reinforcing bar measured by a B-scan. To preserve high resolution and sensitivity to reinforcing bars, 801 sample points across an ultra-wide frequency band from 2.9 GHz to 9 GHz are recorded. Each antenna acts as both the transmitter and receiver. Due to the limited ports of our VNA, the signals are collected by manually connecting each antenna to the VNA channels. The process is repeated until the data received by all antennas have been collected. The data collection process can be accelerated using a multiport switch [29]. After the 15 × 15 full matrix data are acquired in the frequency domain, they are transformed to the time domain via the inverse Fourier Transform. To remove the direct coupling of antennas and the surface reflection, background signals are measured by placing the array on the regions that are far from the reinforcing bars, and then they are subtracted from the measured full-matrix data.

4.3. Experimental results

The diffraction stacking algorithm is applied to image the acquired full-matrix MIMO GPR data. The wave velocity in concrete was estimated based on the backwall reflection. The experimental imaging results of reinforcing bars with different diameters and cover depths are shown in Figs. 11(a)–11(c) and 11(d)–11(f), respectively.

The 3 dB drop technique is used for characterizing the chord length of the reinforcing bar, as shown in Fig. 11. The diameters of reinforcing bars calculated by the proposed sizing method are listed in Table 4. It can be seen that the errors of the estimated reinforcing bar diameters are less than 6% in all cases. The measured results demonstrate that the proposed method maintains its high accuracy when sizing reinforcing bar diameters in real cases.

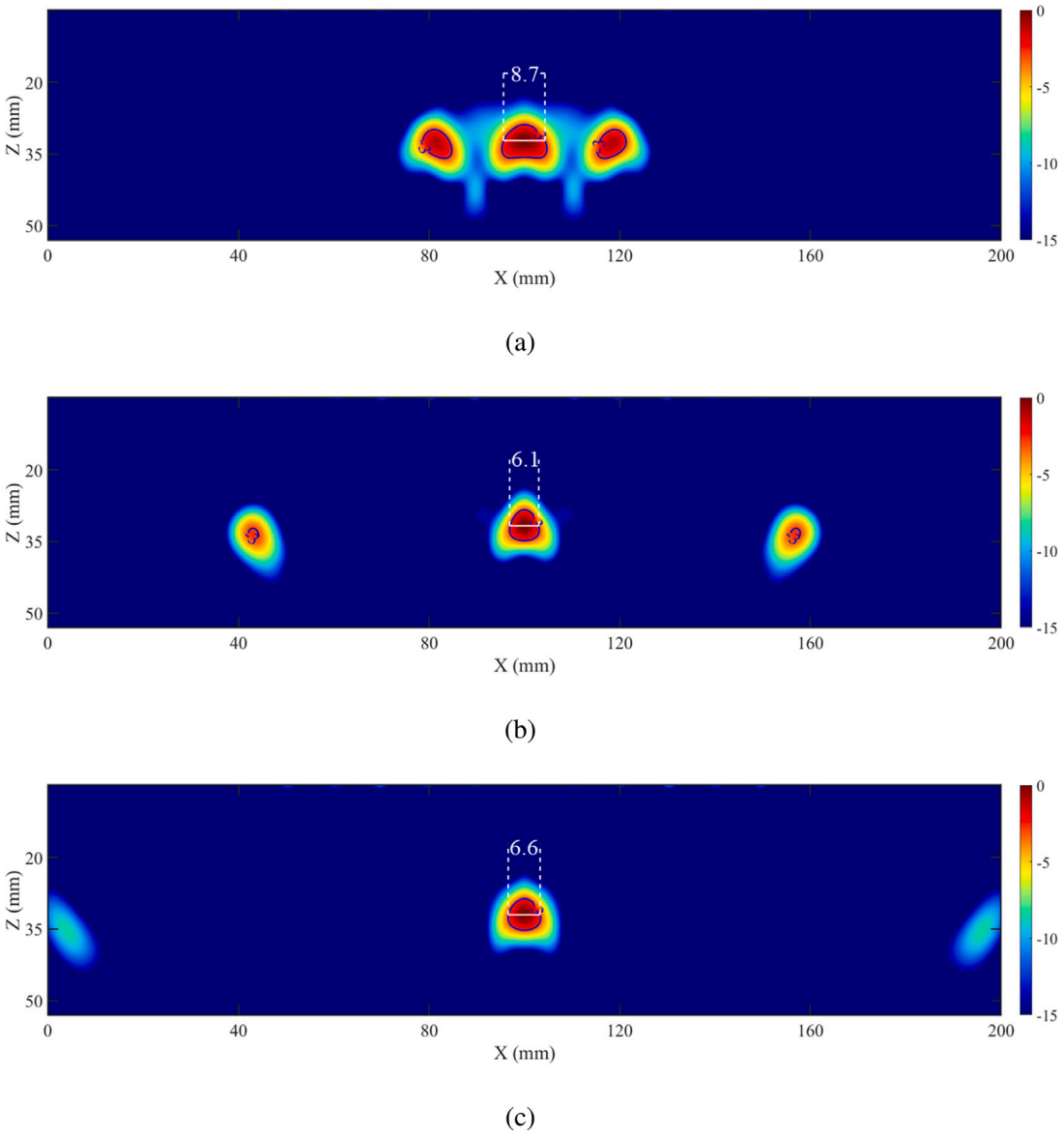

Fig. 8. Diffraction stacking migration imaging results for simulated concrete models including three reinforcing bars with different spacing of (a) 20 mm, (b) 60 mm, and (c) 100 mm.

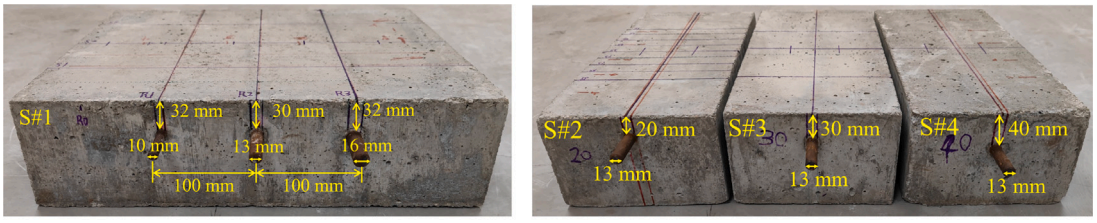

Fig. 9. Test concrete specimens: (a) Specimen S#1 with three reinforcing bars with diameters of 10 mm, 13 mm, and 16 mm, and at a cover depth around 30 mm. (b) Single reinforcing bar with a diameter of 13 mm embedded in three specimens S#2, S#3, S#4 at cover depths of 20 mm, 30 mm, and 40 mm, respectively.

5. Conclusion

In this study, we present a method for estimating the diameter of the reinforcing bar using the MIMO GPR array. The method uses a linear array of UWB antennas to acquire the full-matrix MIMO data, and then applies the diffraction stacking algorithm to reconstruct the image of the reinforcing bars. The diameters of the reinforcing bars are measured based on the cover depth and the chord length that is determined by the 3 dB drop technique. Both numerical simulations and experiments have demonstrated that our method has excellent sizing accuracy with less than 10% error for reinforcing bars with different diameters, and cover depths, even when the alignment of the

Table 4
Experimental validation for the sizing of reinforcing bars with different diameters and cover depths.

Sample	Actual diameter (mm)	Estimated diameter (mm)	Reconstruction error (%)
D10H32(S#1)	10	10.2	2.01%
D13H30(S#1)	13	13.52	4%
D16H32(S#1)	16	16.77	4.8%
D13H20(S#2)	13	13.34	2.6%
D13H30(S#3)	13	13.76	5.86%
D13H40(S#4)	13	13.05	0.38%

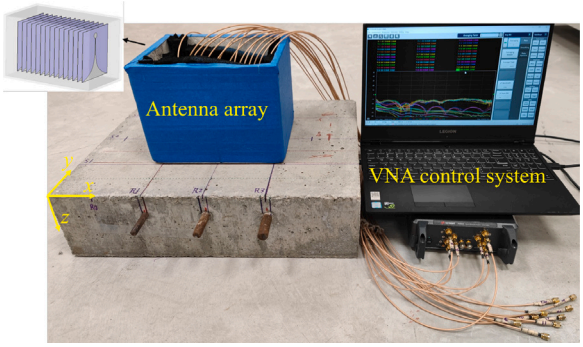

Fig. 10. Experimental setup of the MIMO GPR array measurement using a stepped-frequency GPR control system with a linear array including 15 *y*-polarization Vivaldi antennas.

array is not perfect. The diameter of reinforcing bars is an important indicator to reflect the health status of reinforced buildings. Therefore, our proposed method with its high sizing accuracy can greatly facilitate the health inspection of reinforced buildings. In addition, the promising sizing accuracy achieved in the work can provide insights into further investigation of MIMO GPR systems for accurately sizing subsurface objects in various applications.

It should be noted that the proposed sizing method is demonstrated on the cylindrical reinforcing bars. However, in a real scenario, reinforcing bars may have complex shapes due to the corrosion damage, leading to compromised reconstruction results. This would be investigated in the future work.

CRediT authorship contribution statement

Weixia Cheng: Methodology, Software, Investigation, Data curation, Writing – original draft. **Hai-Han Sun:** Methodology, Investigation, Writing – review & editing. **Kang Hai Tan:** Writing – review & editing, Supervision. **Zheng Fan:** Conceptualization, Writing – review & editing, Supervision.

Declaration of competing interest

The authors declare that they have no known competing financial interests or personal relationships that could have appeared to influence the work reported in this paper.

Data availability

Data will be made available on request.

Acknowledgements

The authors acknowledge funding from A*STAR Science and Engineering Research Council, Singapore under AME Individual Research Grant (IRG) 2018 Grant Call (Project No. A1983c0030).

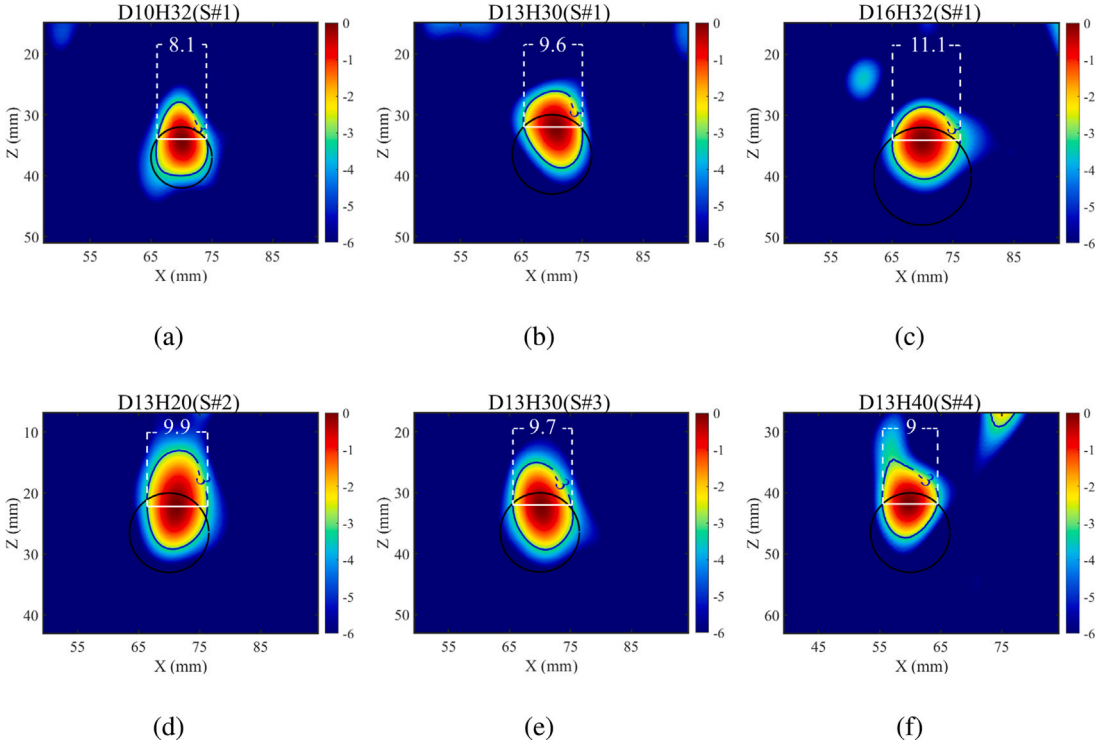

Fig. 11. Imaging results of experimental concrete specimens using the diffraction stacking algorithm: (a)–(c) reinforcing bars with diameters of 10 mm, 13 mm, and 16 mm, and at a cover depth around 30 mm in S#1; (d)–(f) reinforcing bars with a diameter of 13 mm at cover depths of 20 mm, 30 mm, and 40 mm in S#2, S#3, S#4, respectively. D and H in the figures denote the diameter and the cover depth, respectively.

References

[1] J.G. Cabrera, Deterioration of concrete due to reinforcement steel corrosion, Cem. Concr. Compos. 18 (1) (1996) 47–59.

[2] J.P. Broomfield, Corrosion of Steel in Concrete: Understanding, Investigation and Repair, CRC Press, 2003.

[3] C. Fang, K. Lundgren, L. Chen, C. Zhu, Corrosion influence on bond in reinforced concrete, Cem. Concr. Res. 34 (11) (2004) 2159–2167.

[4] H. Liu, J. Zhong, F. Ding, X. Meng, C. Liu, J. Cui, Detection of early-stage rebar corrosion using a polarimetric ground penetrating radar system, Constr. Build. Mater. 317 (2022) 125768.

[5] D.M. McCann, M.C. Forde, Review of NDT methods in the assessment of concrete and masonry structures, NDT E Int. 34 (2) (2001) 71–84.

[6] X.Q. He, Z.Q. Zhu, Q.Y. Liu, G.Y. Lu, Review of GPR rebar detection, in: Prog. Electromagn. Res. Symp., Vol. 1, 2009, pp. 790–799.

[7] H.-H. Sun, Y.H. Lee, W. Luo, L.F. Ow, M.L.M. Yusof, A.C. Yucel, Dual-cross-polarized gpr measurement method for detection and orientation estimation of shallowly buried elongated object, IEEE Trans. Instrum. Meas. 70 (2021) 1–12.

[8] K. Agred, G. Klysz, J.-P. Balayssac, Location of reinforcement and moisture assessment in reinforced concrete with a double receiver gpr antenna, Constr. Build. Mater. 188 (2018) 1119–1127.

[9] M. Rasol, J.C. Pais, V. Pérez-Gracia, M. Solla, F.M. Fernandes, S. Fontul, D. Ayala-Cabrera, F. Schmidt, H. Assadollahi, Gpr monitoring for road transport infrastructure: A systematic review and machine learning insights, Constr. Build. Mater. 324 (2022) 126686.

[10] S. Shihab, W. Al-Nuaimy, Radius estimation for cylindrical objects detected by ground penetrating radar, Subsurf. Sens. Technol. Appl. 6 (2) (2005) 151–166.

[11] A. Dolgiy, A. Dolgiy, V. Zolotarev, Optimal radius estimation for subsurface pipes detected by ground penetrating radar, in: 11th International Conference on Ground Penetrating Radar, 2006, pp. 19–22, (1).

[12] A.V. Ristic, D. Petrovacki, M. Govedarica, A new method to simultaneously estimate the radius of a cylindrical object and the wave propagation velocity from GPR data, Comput. Geosci. 35 (8) (2009) 1620–1630.

[13] Z. Mechbal, A. Khamlichi, Determination of concrete rebars characteristics by enhanced post-processing of gpr scan raw data, NDT Int. 89 (2017) 30–39.

[14] C. Windsor, L. Capineri, Automated object positioning from ground penetrating radar images, Insight 40 (7) (1998) 482–488.

[15] C. Windsor, L. Capineri, P. Falorni, S. Matucci, G. Borgioli, The estimation of buried pipe diameters using ground penetrating radar, Insight Non-Destr. Test. Cond. Monit. 47 (7) (2005) 394–399.

[16] C.G. Windsor, L. Capineri, P. Falorni, A data pair-labeled generalized hough transform for radar location of buried objects, IEEE Geosci. Remote Sens. Lett. 11 (1) (2014) 124–127.

[17] S. Jazayeri, S. Kruse, I. Hasan, N. Yazdani, Reinforced concrete mapping using full-waveform inversion of GPR data, Constr. Build. Mater. 229 (2019) 117102.

[18] X. Li, H. Liu, F. Zhou, Z. Chen, I. Giannakis, E. Slob, Deep learning–based nondestructive evaluation of reinforcement bars using ground-penetrating radar and electromagnetic induction data, Comput. Aided Civ. Infrastruct. Eng. (2021) 1–20.

[19] V. Utsi, E. Utsi, Measurement of reinforcement bar depths and diameters in concrete, in: Proceedings of the Tenth International Conference Ground Penetrating Radar, GPR 2004, Vol. 2, 2004, pp. 659–662.

[20] G. Leucci, Ground penetrating radar: an application to estimate volumetric water content and reinforced bar diameter in concrete structures, J. Adv. Concr. Technol. 10 (12) (2012) 411–422.

[21] L. Zanzi, D. Arosio, Sensitivity and accuracy in rebar diameter measurements from dual-polarized GPR data, Constr. Build. Mater. 48 (2013) 1293–1301.

[22] S. Park, J. Kim, K. Jeon, J. Kim, S. Park, Improvement of gpr-based rebar diameter estimation using yolo-v3, Remote Sens. 13 (10) (2021).

[23] I. Giannakis, A. Giannopoulos, C. Warren, A machine learning scheme for estimating the diameter of reinforcing bars using ground penetrating radar, IEEE Geosci. Remote Sens. Lett. 18 (3) (2021) 461–465.

[24] A. Martinez-Vazquez, J. Fortuny-Guasch, Uwb mimo radar arrays for small area surveillance applications, in: The Second European Conference on Antennas and Propagation, EuCAP 2007, IET, 2007, pp. 1–6.

[25] T. Savelyev, X. Zhuge, A. Yarovoy, L. Ligthart, B. Levitas, Comparison of uwb sar and mimo-based short-range imaging radars, in: 2009 European Radar Conference (EuRAD), IEEE, 2009, pp. 109–112.

[26] A. Srivastav, P. Nguyen, M. McConnell, K.A. Loparo, S. Mandal, A highly digital multiantenna ground-penetrating radar (gpr) system, IEEE Trans. Instrum. Meas. 69 (10) (2020) 7422–7436.

[27] Z. Liang, Q. Liu, T. Long, A novel subarray digital modulation technique for wideband phased array radar, IEEE Trans. Instrum. Meas. 69 (10) (2020) 7365–7376.

[28] E.M. Johansson, J.E. Mast, Three-dimensional ground-penetrating radar imaging using synthetic aperture time-domain focusing, Adv. Microw. Millim. Wave Detect. 2275 (September 1994) (1994) 205–214.

[29] A.G. Yarovoy, T.G. Savelyev, P.J. Aubry, P.E. Lys, L.P. Ligthart, Uwb arraybased sensor for near-field imaging, IEEE Trans. Microw. Theory Tech. 55 (6) (2007) 1288–1295.

[30] Y. Li, W. Lu, G. Fang, B. Zhou, S. Shen, Performance verification of Lunar Regolith Penetrating Array Radar of Chang'E-5 mission, Adv. Space Res. 63 (7) (2019) 2267–2278.

[31] X. Zhuge, A.G. Yarovoy, T. Savelyev, L. Ligthart, Modified kirchhoff migration for UWB MIMO array-based radar imaging, IEEE Trans. Geosci. Remote Sens. 48 (6) (2010) 2692–2703.

[32] D.H. Marpaung, Y. Lu, A comparative study of migration algorithms for UWB GPR images in SISO-SAR and MIMO-array configurations, in: Proc. Int. Radar Symp., 2014.

[33] D.H.N. Marpaung, Y. Lu, Autofocusing of uwb mimo gpr images by using mzo and entropy minimization, IEEE Geosci. Remote Sens. Lett. 13 (5) (2016) 661–665.

[34] H. Liu, Z. Long, C. Qiu, F. Han, Q.H. Liu, Reverse-time migration and full wavefrom inversion for subsurface imaging, in: 2016 Progress in Electromagnetic Research Symposium, PIERS, 2016, p. 149.

[35] H. Liu, Z. Long, B. Tian, F. Han, G. Fang, Q.H. Liu, Two-dimensional reverse-time migration applied to GPR with a 3-D-to-2-D data conversion, IEEE J. Sel. Top. Appl. Earth Obs. Remote Sens. 10 (10) (2017) 4313–4320.

[36] D.B. Miron, Chapter 2 - Antenna fundamentals I, in: D.B. Miron (Ed.), Small Antenna Design, Newnes, Burlington, 2006, pp. 9–41.

[37] M. Moles, Defect sizing in pipeline welds: What can we really achieve? in: ASME Pressure Vessels and Piping Conference, Vol. 46792, 2004, pp. 31–39.

[38] I.L. Al-Qadi, S. Lahouar, Measuring rebar cover depth in rigid pavements with ground-penetrating radar, Transp. Res. Rec. 1907 (1) (2005) 80–85.

[39] C. Warren, A. Giannopoulos, I. Giannakis, gprMax: Open source software to simulate electromagnetic wave propagation for Ground Penetrating Radar, Comput. Phys. Comm. 209 (2016) 163–170.

[40] C. Warren, A. Giannopoulos, A. Gray, I. Giannakis, A. Patterson, L. Wetter, A. Hamrah, A CUDA-based GPU engine for gprMax: Open source FDTD electromagnetic simulation software, Comput. Phys. Comm. 237 (2019) 208–218.

[41] E. 1992-1-1, Eurocode 2: Design of Concrete Structures - Part 1-1 : General Rules and Rules for Buildings, European Committee for Standardization (CEN), Brussels, Belgium, 2004.

[42] S.-Y. Hyun, J.-K. Du, H.-J. Lee, K.-W. Lee, J.-H. Lee, C. Jung, E.-J. Kim, W. Kim, J.-G. Yook, Analysis of shielding effectiveness of reinforced concrete against high-altitude electromagnetic pulse, IEEE Trans. Electromagn. Compat. 56 (6) (2014) 1488–1496.

[43] H. Liu, H. Lu, J. Lin, F. Han, C. Liu, J. Cui, B.F. Spencer, Penetration properties of ground penetrating radar waves through rebar grids, IEEE Geosci. Remote Sens. Lett. 18 (7) (2020) 1199–1203.